To IMAGE or to IMAGINE: visualization of parasite migration as a means to support (malaria) parasite vaccine development

Korne, C.M. de


5

A hybrid tracer approach reveals the in vivo dissemination kinetics of syringe-injected malaria sporozoites

Clarize M. de Korne, Mick M. Welling, Danny M. van Willigen, Fabian W. Hensbergen, Severine C. Chevalley-Maurel, Jeroen C. Sijtsma, Roos van Schuijlenburg, Els Baalbergen, Blandine M.D. Franke-Fayard, Meta Roestenberg, Fijs W.B. van Leeuwen

Unpublished

ABSTRACT

Malaria sporozoites (SPZ) present the first stage of a malaria infection. Following release during a mosquito bite, SPZ actively migrate from the skin to the liver to initiate the next stage of their life cycle. Currently, one of the leading vaccine candidates to prevent malaria are live-attenuated SPZ administered intravenously by syringe (PfSPZ Vaccine, Sanaria). Preclinical and clinical data indicate that the way of administration is essential to determine the overall potency of SPZ-based vaccine candidates. While it is known that accumulation of SPZ in the liver is key, little is known about the dissemination kinetics of these SPZ vaccines following injection and the role of SPZ motility in this process. To obtain such insights, SPZ need to be labeled to allow for whole-body tracking. Based on our previous experience with SPZ tracking in skin using a fluorescent tracer, we have now developed a radiolabeled analogue (^{99m}Tc-Cy5-AmineC4.MAS$_3$-Methyl) that was used to quantify SPZ dissemination in a murine model. The fluorescent signature of the tracer was used to confirm the labeling of the SPZ by microscopy and flow cytometry. We found that 2 hr post injection live SPZ mainly distributed towards the liver. This contrasted the biodistribution of non-viable and thus non-motile SPZ, which showed a lower liver-to-lungs distribution as compared to their live counterparts. These findings suggest that SPZ viability is critical for them to pass the lungs and migrate to the liver. Further research is needed to improve the specificity of the labeling and thereby reduce the background signal found in this study. Nevertheless, in this proof-of-concept study the first hybrid tracer-based labeling approach for SPZ has been developed and tested, enabling investigation of the spatial and temporal dynamics of (vaccine) SPZ throughout their host.

INTRODUCTION

The initial progress made in malaria control during the first two decades of the 21st century has come to a halt, and as a result malaria cases are resurging and malaria remains responsible for over 500.000 deaths every year[1]. A pressing need remains for novel control tools such as malaria vaccines. During the initial stage of a malaria infection, the mosquito-inoculated parasites called sporozoites (SPZ) are still low in number (1-500 per mosquito bite) and vulnerable to immune attack[2-5]. As a consequence, vaccine researchers have turned to exploiting the use of whole SPZ or SPZ proteins as vaccines. Live-attenuated whole SPZ vaccines have shown potential in providing 50-100% protection to adults in clinical trials and thus are currently leading vaccine candidates in the prevention of malaria[6-8].

Remarkably, the potency of vaccine SPZ is determined by the way they are administered, raising the hypothesis that SPZ biodistribution is of importance in the protection induced by SPZ. Dose-escalation studies showed that intradermal administration protected at best 2/16 (13%) volunteers against a controlled human malaria infection while intravenous administration induced protection in 12/15 (80%) volunteers at high doses[9, 10].

Despite the fact that the location of SPZ and their interactions with immune cells at these different locations seem to be critical for the vaccine-induced protective immune response[11], only a little is known about the migration patterns of live, attenuated vaccine SPZ. After intradermal mosquito-inoculation in rodents, SPZ aim to enter the circulatory system to get transported to the liver where they invade hepatocytes and multiply[12]. Initial studies into the migration patterns of mosquito-inoculated SPZ revealed that the majority of SPZ remain for at least several hours in the skin and some are trapped in lymphatic vessels[13, 14]. However, studies into the distribution of vaccine SPZ administered by injection have not been performed. A better understanding of the distribution of SPZ throughout the host following injection would help to understand where immune interactions can take place and thus aid the development of an efficacious malaria vaccine.

Investigations into the biodistribution of SPZ is hampered by the lack of a method that enables whole-body, longitudinal tracking of SPZ. SPZ migration has been extensively studied in murine and human skin using fluorescence-based tracking. This method is sensitive enough to track single SPZ under the condition of a micrometer-scale field of view[13, 15-17], but this sensitivity is lost when zooming out to whole-body scale due to the limited penetration depth of fluorescence signal in tissue. Longitudinal tracking of malaria parasites has so far only been done using the parasite's blood stages in mice. To make this possible, bioluminescence imaging is used, which will detect parasites provided that their numbers are high enough to reach the detection threshold[18, 19]. However, this method is not sensitive enough to track the low numbers of parasites during the SPZ stage.

Although not applied in the field of parasitology yet, tracking of low numbers of cells, e.g. T cells and stem cells, migrating throughout the body is achieved in other research fields using the sensitivity, quantifiability and tissue penetration capacity of radioactivity[20-22]. For example, a clinical standard for detecting inflammatory lesions makes use of radiolabeled white blood cells[23]. Recently, we have developed a fluorescent cyanine dye-based tracer suitable to label SPZ by targeting their mitochondrion and subsequently track them in skin[24].

In this study, we report a preliminary assessment of SPZ dissemination following intravenous injection using the mitochondrial tracer ^{99m}Tc-Cy5-Methyl-AmineC4.MAS$_3$ (^{99m}Cy5-MAS$_3$). We performed biodistribution studies of radiolabeled viable and non-viable SPZ using a murine model. Hereby we exploit both the fluorescent and radioactive signature of the tracer. As far as we are aware, this is the first study that provides a proof of concept for the radiolabeling of SPZ that enables whole-body *in vivo* tracking. We were able to gain insights in the role of SPZ viability in their dissemination throughout the host, especially regarding lung passage.

METHODS

Tracer synthesis

Cy5-AmineC4.MAS$_3$-Methyl was synthesized and characterized as described in the Supplementary Information. In brief, the chelate mercaptoacetyltriserine (MAS$_3$) was coupled to Cy5-Methyl-AmineC4 by forming an amide bond, yielding the tracer Cy5- AmineC4.MAS$_3$-Methyl (from now abbreviated as Cy5-MAS$_3$). The crude compound was purified using preparative-scale prep-HPLC (high-performance liquid chromatography) and the product structure was confirmed by NMR (nuclear magnetic resonance) spectroscopy. Subsequently, the (photo)physical properties of the tracer were assessed; the molar extinction coefficient (ε) and quantum yield (ΦF) were assessed to calculate the brightness (ε*ΦF) and the lipophilicity (log P) and serum binding were determined as previously described[25].

Radiolabeling of Cy5-MAS$_3$

Radiolabeling of Cy5-MAS$_3$ with technetium-99m was performed according to a previously described protocol with some minor amendments[26]. To Cy5-MAS$_3$, 80 or 250 MBq technetium-99m (80 Mbq for biodistribution of free tracer, 250 Mbq for radiolabeling of SPZ) freshly eluted from a generator (~1 GBq/ml; Ultra-Technekow™, Mallinckrodt Medical B.V.) was added to a mixture containing 0.5 nmol of the tracer (992 µM stock in H_2O) and the following buffer solutions: 10.5 µl of phosphate buffer (0.5 M, pH 8), 15.6 µl of phosphate buffer (0.25 M, pH 8), 12.5 µl disodium tartrate dihydrate (50 mg/mL in phosphate buffer (0.5 M, pH 8)) and 3.1 µl of Tin(II) chloride dihydrate (4 mg/ml in L-ascorbic acid solution (3 mg/ml in 0.1 M HCl)) (Sigma-Aldrich). The Tin(II) chloride dihydrate solution was freshly

prepared and N_2 degassed for 20 minutes, all other buffers were prepared and stored at 4°C for maximally 1 month. After heating to 100°C for 20 minutes, the reaction mixture was cooled down to room temperature and diluted with 10 ml Milli-Q water. This solution was passed through a Sep-Pak C-18 cartridge (Waters) pre-rinsed with EtOH, followed by another 10 ml of Milli-Q water. After that, the labeled tracer was drop-wise eluted from the cartridge with EtOH into the reaction tube followed by vigorous vortexing. The volume of this eluate was reduced to 10 µl by evaporation of ethanol. The radiochemical purity of the final product ^{99m}Tc-Cy5-MAS$_3$ was analyzed by radio-thin layer chromatography (radio-TLC; Supelco) using acetonitrile as mobile phase.

Rodent experiments

All animal experiments were granted a license by the Competent Authority after advice by the Animal Experiments Committee Leiden (AVD1160020173304). All experiments were performed in accordance with the Experiments on Animals Act (Wod, 2014), the applicable legislation in the Netherlands, and in accordance with the European guidelines (EU directive no. 2010/63/EU) regarding the protection of animals used for scientific purposes. All experiments were performed in a licensed establishment for the use of experimental animals (LUMC). For this study we used female Swiss OF1 mice (6-7 weeks old; Charles River) that were housed in individually ventilated cages furnished with autoclaved aspen woodchip, fun tunnel, wood chew block and nestlets at 21 ± 2°C under a 12:12 hr light-dark cycle at a relative humidity of 55 ± 10%.

***Plasmodium* sporozoite production**

Naive mice were infected with the rodent malaria species *Plasmodium berghei* as described previously[27]. The transgenic line 1868cl1 expressing mCherry and luciferase under the constitutive HSP70 and eef1a promotors respectively (*Pb*ANKA-mCherry$_{hsp70}$+Luc$_{eef1\alpha}$; line RMgm-1320, www.pberghei.eu) was used. The infected mice were anesthetized and *Anopheles stephensi* female mosquitoes were infected by feeding on the gametocytemic mice. The mosquitoes were kept at a temperature of 21 °C and 80% humidity until dissection. SPZ were obtained by manual dissection of the salivary glands of the infected mosquitoes 20-24 days post infection. The salivary glands were collected and homogenized to release SPZ in Roswell Park Memorial Institute medium (RPMI; Thermo Fisher Scientific) enriched with 10% fetal bovine serum (FBS; Life Technologies Inc.). The free SPZ were counted in a Bürker counting chamber using phase-contrast microscopy and thereafter, within 1 hr, the labeling of the SPZ was initiated. To obtain salivary gland material (SGM), the salivary glands of uninfected mosquitoes were collected and homogenized in RPMI + 10%FBS.

Labeling of sporozoites

To label isolated SPZ with Cy5-MAS$_3$ or ^{99m}Tc-Cy5-MAS$_3$, 0.5 nmol tracer in 10 µl EtOH was

added to $1.0*10^6$ SPZ in 990 µl RPMI + 10% FBS. The mixture was gently stirred at room temperature for 30 minutes. The SPZ were then purified by 3 consecutive wash steps; 5 minutes centrifugation at 7,200 x g, followed by decanting and adding 1.5 ml RPMI + 10% FBS. Critical in this process was to reduce the amount of unbound tracer by >99.99% while preserving SPZ viability. After the labeling, the SPZ were recounted. To obtain non-viable labeled SPZ, the viable radiolabeled SPZ were fixed for 20 minutes with 4% paraformaldehyde (Thermo Fisher Scientific). This was done in between the first and the second wash step. The viability of the live/non-viable SPZ was validated by measuring the bioluminescent signal by a GloMax plate reader (Promega) after adding cell culture lysis reagent and luciferase assay reagent (Promega) following the manufacturer's instruction.

Sporozoite labeling stability and dissociation

To study the labeling stability, SPZ labeled with Cy5-MAS_3 were pipetted on the coverslip of a confocal dish without any precoating (ø14mm; MatTek Corporation), covered and microscopically analyzed. Images of the SPZ were taken using an Andor Dragonfly 500 spinning disk confocal on a Leica DMi8 microscope (Oxford Instruments) combined with the Andor imaging software Fusion (Oxford Instruments). The mCherry expressed by SPZ was excited with the 561 nm laser and the Cy5-MAS_3 tracer was excited with the 637 nm laser. The fluorescent intensity of SPZ labeled with Cy5-MAS_3 was also evaluated using a flow cytometer (BD LSR Fortessa 4L; BD Bioscience and Cytek Aurora; Cytek Biosciences). The data was analyzed using the FlowJo software (FlowJo LLC). SPZ were selected by gating on mCherry-positive events, and per SPZ, the mean fluorescent intensity of the Cy5-MAS_3 labeling was quantified. To determine the dissociation of the ^{99m}Tc-Cy5-MAS_3 from SPZ over time, at various intervals up to 24 hr after labeling, SPZ labeled with ^{99m}Tc-Cy5-MAS_3 were filtered (Millex-HV syringe filter unit, 0.2 µm; Millipore), the radioactivity in the filtrate was measured with a gamma counter (Wizard2 2470 automatic gamma scintillation counter; PerkinElmer) and the percentage decrease of SPZ-bound tracer was calculated by comparing the amount of radioactivity in the filtrate with the amount of radioactivity in a non-filtered sample. As a control, SGM was labeled and the stability of the labeling was determined according to the same protocol.

Sporozoite motility assessment

The motility of the SPZ labeled with Cy5-MAS_3 was assessed *in vitro* as described previously[28] and was compared to the motility of non-labeled SPZ. The SPZ were pipetted on the coverslip of a confocal dish and covered. Movies of their circular movement pattern were recorded on a Leica TCS (true confocal scanning) SP5 microscope (Leica Microsystems, Wetzlar) combined with Leica imaging software (Leica Microsystems, Wetzlar). The mCherry expressed by SPZ was excited with the 561 nm laser and the emission signal was collected between 600-650 nm. The movies were recorded with a frame rate of 35 frames per minute,

200 frames per movie. Maximum projections of the recorded microscopy movies were generated using Fiji software[29]. The movies were further processed using $SMOOT_{in\ vitro}$, an in-house developed graphical user interface (GUI), written in the MATLAB programming environment (The MathWorks Inc.)[28]. The movement pattern of the SPZ was classified as floating, stationary or circling and the velocity of the circling SPZ was determined. In total, the motility of 379 SPZ was analyzed, distributed over the labeled (n=178) and control (n=201) condition.

Infectivity labeled sporozoites

The infectivity of the SPZ labeled with Cy5-MAS_3 was assessed *in vitro* and *in vivo* and compared to the infectivity of non-labeled SPZ. For *in vitro* assessment, Huh-7 cells (immortal human hepatoma cell line) were seeded into a 24-well plate at $5*10^4$ cells/well and kept overnight in RPMI + 10% FBS at 37°C in a humidified atmosphere with 5% CO_2. SPZ were added to the hepatocytes in a 1:1 ratio. Live imaging of liver-stage parasite development (presence of liver schizonts) was performed 44 hr after the addition of the SPZ using a conventional fluorescent microscope (Leica AF6000LX, Oxford Instruments). The nuclei of the cells were stained using Hoechst 33342 (1:200; 1 mg/ml; Sigma-Aldrich). The mCherry expressed by the schizonts was excited with the 561 nm laser and Hoechst was excited with the 405 nm UV laser. After imaging, the medium was removed and the cells were incubated for 5 minutes with cell culture lysis reagent. Subsequently, luciferase assay reagent was added to the lysed cells and the bioluminescence signal was measured by a GloMax plate reader.

To assess the infectivity of the labeled SPZ *in vivo*, $5*10^4$ SPZ in 200 µl medium were injected intravenously into the tail vein of mice (n=6 for labeled SPZ, n=6 for non-labeled SPZ) using an insulin syringe (Micro-Fine+, 0.5 ml, 0.30 x 8.0 mm, 30G; Becton Dickinson). The parasite liver load was visualized and quantified by measuring the luciferase activity in the liver at 44 hr after the challenge with SPZ using the IVIS Lumina II (Perkin Elmer Life Sciences). Animals were kept anesthetized during the measurements using the isoflurane-anesthesia system (XGI-8, Caliper Life Sciences). IVIS measurements (exposure time: 60 seconds, binning factor: 8, aperture: f/1) were performed 8 minutes after subcutaneously injection of D-luciferin in the neck (100 mg/kg in PBS; Caliper Life Sciences). The liver load was quantified by measuring the total flux (p/s) of an ROI covering the liver (same ROI for all mice). Image analysis was performed using the Living Image® 4.4 software (Perkin Elmer Life Sciences). Infected mice were monitored for blood-stage infections by Giemsa-stained blood smear at day 5 to 14 post infection. The prepatent period (measured in days after SPZ injection) was defined as the first day at which blood-stage infection with a parasitemia of >0.5% was observed.

Biodistribution of ^{99m}Tc-Cy5-MAS$_3$

The biodistribution of the free tracer ^{99m}Tc-Cy5-MAS$_3$ was determined 2 hr after intravenous (IV) administration. For IV injection, 200 µl medium containing 0.5 nmol of ^{99m}Tc-Cy5-MAS$_3$ (45±8 MBq) was injected into the tail vein of the mice (n=6) using an insulin syringe. Animals were kept anesthetized during the injections using the isoflurane-anesthesia system. The total injected dose was determined by counting full and empty syringes in a gamma counter (2470 automatic gamma counter, Perkin–Elmer) or by counting the whole mouse in the gamma counter directly post injection. To obtain a total body SPECT scan at 2 hr post injection, the mice were placed onto a dedicated positioning bed of a three-headed U-SPECT-2 (MILabs) under continuous isoflurane anesthesia and radioactivity counts from total body scans were acquired for 18 min on the 140-keV photopeak with a 20% symmetrical window. The projections were reconstructed as described before[30]. Reconstructed images were generated using MATLAB software (The MathWorks Inc.). After imaging, blood was collected by heart puncture and the mice were euthanized by cervical dislocation. The organs of the mice were harvested and weighed. To determine the biodistribution of the tracer, the organs were scanned for fluorescence by IVIS and counted for radioactivity in a gamma counter (Wizard2 2470 automatic gamma scintillation counter, Perkin Elmer). After excision of the tissues, the total amount of remaining radioactivity in the animal carcass was counted. Radioactive counts in tissues were expressed as the percentage of the total injected dose of radioactivity (%ID, corrected for radioisotope decay) or %ID per gram of tissue (%ID/g).

Biodistribution of sporozoites

The biodistribution of SPZ labeled with ^{99m}Tc-Cy5-MAS$_3$ was determined 2 hr post injection under 2 different conditions: 1) 200 µl medium containing $0.5*10^6$ live SPZ was IV injected into the tail vein of the mice using an insulin syringe (n=6), 2) 200 µl medium containing $0.5*10^6$ non-viable SPZ was IV injected into the tail vein of the mice using an insulin syringe (n=6). As a control, 200 µl medium containing the estimated amount of radiolabeled SGM present in a sample containing $0.5*10^6$ SPZ was IV injected into the tail vein of the mice using an insulin syringe (n=9). Animals were kept anesthetized during the injections using the isoflurane-anesthesia system. The total injected dose was determined by counting full and empty syringes in a gamma counter. At 2 hr post injection, blood was collected by heart puncture and the mice were euthanized by cervical dislocation. The organs of the mice were harvested, weighed and counted in a gamma counter (Wizard2 2470 automatic gamma scintillation counter, Perkin Elmer). After excision of the tissues, the remaining radioactivity in the animal carcass was determined. Radioactive counts in tissues were expressed as the percentage of the total injected dose of radioactivity (%ID, corrected for decay) or %ID per gram of tissue (%ID/g). An overview of the biodistribution results of the different conditions which includes the %ID and %ID/g determined for 16 different tissues has been attached

as Sup. Figure S1. Based on the %ID per organ, the ratio of radioactivity retrieved from the liver to the clearance organs (intestines + gall bladder) and the ratio of radioactivity retrieved from the lungs to the clearance organs were calculated (liver:clearance ratio, lungs:clearance ratio).

Statistics

The average and variability of the data were summarized using the mean and standard deviation (SD) for parametric data or the median and interquartile range (IQR) for nonparametric data. For the comparison of groups, the difference between means or medians was assessed using respectively the independent sample T-test and the Mann-Whitney U test. For the comparison of a group with a set value, the one-sample T-test was used. P-values < 0.05 were considered significant. All statistical tests were performed by SPSS Statistics (IBM Nederland BV).

RESULTS

Sporozoite radiotracer development

A radiotracer suitable to label SPZ was developed by coupling the previous synthesized fluorescent tracer Cy5-Methyl-Methyl[24] to a MAS_3 chelate followed by ^{99m}Tc radiolabeling, yielding the hybrid tracer ^{99m}Tc-Cy5-MAS_3 (Figure 1A). The brightness of the tracer, its most valuable photophysical trait, was $3.45 \cdot 10^3$ $M^{-1} \cdot cm^{-1}$ (the product of its quantum yield $\phi_{F, PBS}$ = 13% and molar extinction coefficient $\varepsilon_{PBS} = 2.65 \cdot 10^4$ $M^{-1} \cdot cm^{-1}$). *In vitro* confocal microscopy of SPZ labeled with Cy5-MAS_3 revealed a similar staining pattern as previously reported for Cy5-Methyl-Methyl[24]; a single fluorescent spot adjacent to the nucleus where the single parasite mitochondrion is located (Figure 1B). Cy5-MAS_3 uptake by SPZ was also quantified by flow cytometry which showed a 8.9-fold increase in mean fluorescence intensity of Cy5-MAS_3 labeled SPZ compared to non-labeled controls (Figure 1C). Microscopic and flow cytometric analyses showed that the tracer accumulated in SPZ and in the residual salivary gland material (SGM) resulting from the isolation of SPZ (Figure 1B, Sup. Figure S2).

Tracer dissociation over time

The radiolabeling of SPZ with ^{99m}Tc-Cy5-MAS_3 yielded an average of 1.4 MBq bound activity per $1*10^6$ SPZ. Directly after washing, the supernatant contained <2% of background signal originating from non-bound tracer. After 2 hr, 10 ± 2% of the bound tracer was released from the SPZ (and the SGM present) versus 24 ± 4% in case of the SGM control (Figure 2). This indicated that the tracer was mainly released from SGM and that the SPZ were stably labeled, which was confirmed by flow cytometry (Sup. Figure S2).

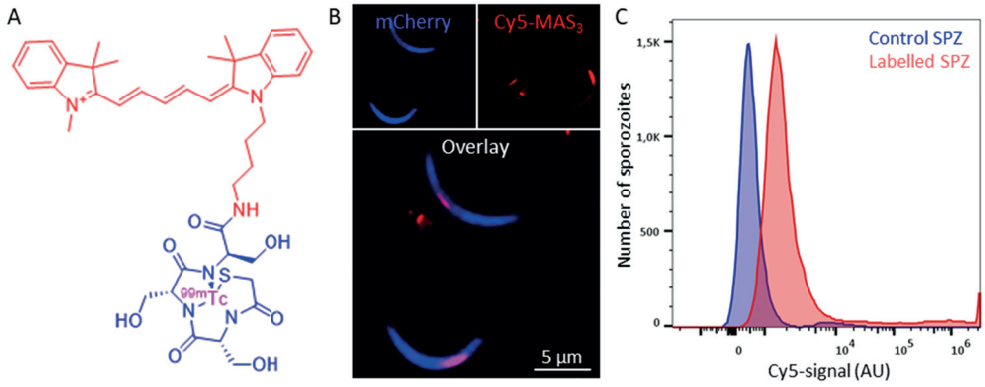

Figure 1 Molecular structure and sporozoite labeling. A) The chemical structure of the hybrid tracer ^{99m}Tc-Cy5-Methyl-AmineC4.MAS$_3$ which contains a Cy5 dye (depicted in red) and a MAS$_3$ chelate (depicted in blue) containing ^{99m}Tc (depicted in pink). B) Microscopic analysis of SPZ expressing mCherry (top left, depicted in blue) labeled with the Cy5-MAS$_3$ tracer (top right, depicted in red), the bottom panel shows the overlay. C) Representative graph of the flow cytometric analysis of the SPZ labeling. Blue lines represent background signal in non-labeled control SPZ, red lines show Cy5 signal in the SPZ labeled with the Cy5-MAS$_3$ tracer.

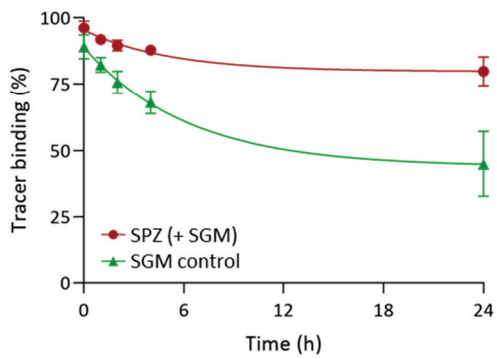

Figure 2 Tracer dissociation. Over time bound tracer was released. The dissociation dynamics are estimated by non-linear fitting using the one phase exponential decay equation and plotted for SPZ (with SGM present) and the SGM control.

Motility and infectivity of labeled sporozoites

The motility of the Cy5-MAS$_3$ labeled SPZ was compared to the motility of non-labeled SPZ using SMOOT$_{in\ vitro}$[28], which is to our knowledge the most sensitive motility analysis tool to detect differences in viability. A representative example of SPZ tracks is shown in Figure 3A. 58% of both labeled and non-labeled SPZ were moving during recording, a third was floating (labeled: 35%, non-labeled: 34%) and a small part was stationary (labeled: 7%, non-labeled: 8%) (p=0.89; Chi-square test) (Figure 3B). The circular movements of both groups had a similar mean velocity (labeled: 2.1 ± 0.8 µm/s, non-labeled: 2.2 ± 0.6 µm/s;

p=0.292, independent sample T test) (Figure 3C). Besides SPZ motility, also their infectivity was assessed both *in vitro* (infection of hepatocytes) and *in vivo* (infection of mice) (Figure 3D-F). 44 hr post infection with labeled SPZ, fully mature liver stages were detected in *in vitro* hepatocytes (Figure 3D) and the livers of mice (Figure 3E). The infectivity of labeled SPZ *in vitro* in hepatocytes was not statistically significantly different, although this assay is known to display high variability (76 ± 44%, 7 independent experiments; p=0.198, one sample T-test). Also *in vivo* there was little difference between infectivity of labeled vs unlabeled SPZ (86 ± 3%, 2 independent experiments; p=0.098, one sample T-test) (Figure 3F). The prepatency of the mice infected with the labeled SPZ was comparable to that of mice infected with non-labeled SPZ, both at 5-6 days after infection. Overall, we concluded that Cy5-MAS$_3$ labeled SPZ were equally capable of migrating, infecting hepatocytes and propagating to blood stage parasites.

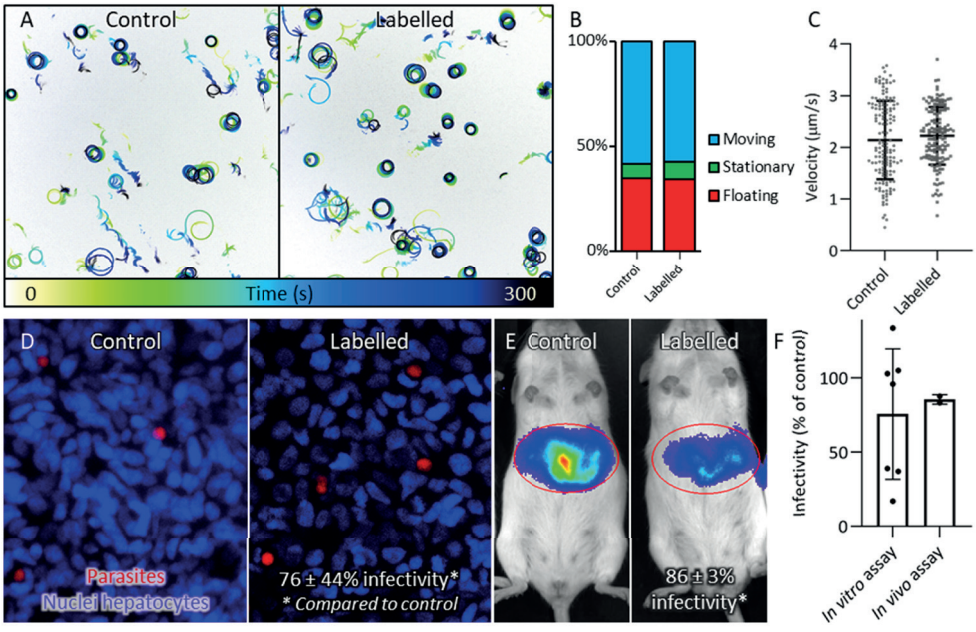

Figure 3 Sporozoite motility and infectivity. A) Overview of the tracks of non-labeled control SPZ and SPZ labeled with Cy5-MAS$_3$. The tracks are color-coded for time. B) The movement pattern distribution of control and labeled SPZ, classified as floating, stationary or moving. C) The mean velocity of the moving control and labeled SPZ. D) The infectivity of control and labeled SPZ is shown as the *in vitro* infection of hepatocytes (parasites are depicted in red, nuclei of hepatocytes in blue). E) The infectivity of control and labeled SPZ is shown as the parasite liver load in mice after 44 hr (bioluminescence signal – median total flux). F) The infectivity of the labeled SPZ is calculated and plotted as a percentage of the infectivity of the control SPZ (middle; the dots represent individual experiments and the error bars represent the SD).

Biodistribution of free tracer and SGM

To be able to investigate the biodistribution results of the labeled SPZ, we first assessed the biodistribution of the free tracer and labeled SGM (Figure 4). Both SPECT imaging and radioactivity biodistribution revealed that, 2 hr after intravenous injection, the free tracer ^{99m}Tc-Cy5-MAS$_3$ mainly accumulated in the gall bladder and the intestines and to a lesser extent in the liver (Figure 4AB). This clearly pointed towards a biliary clearance pathway and subsequent intestinal uptake. Using SGM (particles of varying size around an average of ~2 µm (Sup. Figure S5)), radioactivity was mainly retrieved from the clearance organs (intestines and gall bladder), similar to the free tracer distribution (Figure 4). These results corroborated with prior findings that the tracer rapidly dissociated from SGM (Figure 2). In addition to that, uptake was detected in the liver and the lungs. The signal obtained from the lungs seemed specific for SGM, since the lungs were not a site of accumulation for the free tracer. The signal obtained from the liver may, in part, be attributed to SGM and in part due to free tracer which has been released. This assumption was supported by the notion that the ratio of the clearance organs (intestines + gall bladder) to the liver was larger for SGM (0.41) as compared to the free tracer (0.23). Indicating that roughly half of the signal in the liver came from the labeled SGM (Figure 4B).

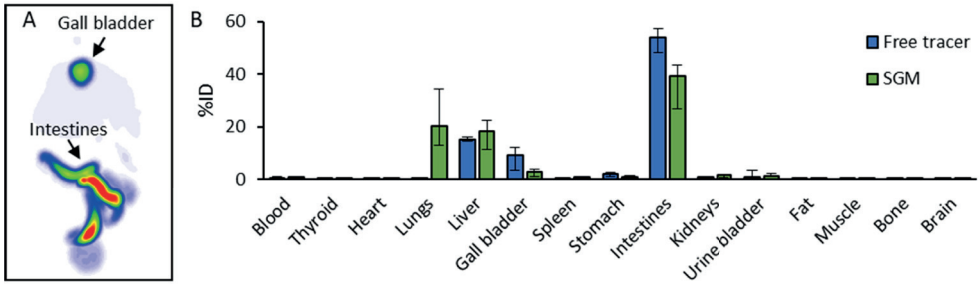

Figure 4 Biodistribution of free tracer and SGM. A) At 2 hr after injection of ^{99m}Tc-Cy5-MAS$_3$, a total body SPECT scan was obtained. B) The biodistribution of the tracer (depicted in light blue) and the biodistribution of SGM labeled with ^{99m}Tc-Cy5-MAS$_3$ (depicted in dark blue) measured 2 hr after injection, plotted as the median percentage of injected dose (%ID) per organ including error bars representing the inter quartile range.

Biodistribution of sporozoites

Radiolabeled SPZ were injected intravenously into the mouse tail vein as depicted in Figure 5A. The biodistribution results (%ID) revealed that 2 hr after intravenous injection, accumulation occurred in the lungs, liver and intestines + gall bladder (Figure 5B). Since SPZ cannot migrate to the bile, this signal and that in the intestines reflected the presence of free tracer (which was cleared via the bile and intestines), which was confirmed by qRT-PCR analysis (Sup. Figure S3). Based on these findings, we calculated the lungs:clearance ratio and

the liver:clearance ratio and compared these to the ratio's obtained for the biodistribution of SGM. The lungs:clearance ratio was comparable, though slightly increased, compared to SGM (lungs:clearance ratio live SPZ: 0.52, SGM: 0.46). However, the liver:clearance ratio of live SPZ was higher compared to the ratio of SGM (liver:clearance ratio live SPZ: 0.62, SGM: 0.41). Indicating that while some SPZ had ended up in the lungs, most had reached the liver, which was confirmed by visualization of liver parasites by microscopy (Sup. Figure S4).

Effect of viability on the biodistribution of sporozoites

To assess the role of SPZ viability in their biodistribution, we compared the biodistribution results of non-viable SPZ to the biodistribution of live SPZ. Two hours after the injection of non-viable radiolabeled SPZ relatively larger amounts of radioactivity were retrieved from the lungs, which was offset by a reciprocal decrease in signal retrieved from the liver (increase in lungs:clearance ratio: +0.21, decrease in liver:clearance ratio: -0.26) (Figure 5C). As such the lack of viability induced a significant shift in radioactivity accumulation from liver to lungs (p=0.025; Mann-Whitney U test). This indicated that live SPZ were better able to pass the lungs and reach the liver than non-viable SPZ.

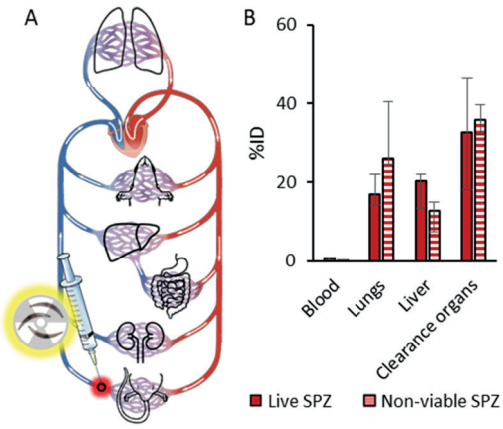

	Lungs:Clearance	Liver:Clearance
Free tracer	0.00	0.23
SGM	0.46	0.41
Live SPZ	0.52	0.62
Non-viable SPZ	0.73	0.36

Figure 5 Biodistribution of intravenously injected live and non-viable sporozoites. A) The intravenous injection route of labeled SPZ is annotated in a schematic overview of the circulatory system. B) The biodistribution results of live (plain red) and non-viable SPZ (striped red) measured 2 hr after injection, plotted as the median percentage of injected dose (%ID) per organ including error bars representing the inter quartile range. Clearance organs: intestines + gall bladder. C) The ratio of signal from the lungs versus the clearance organs (lungs:clearance) and from the liver versus the clearance organs (liver:clearance) was calculated.

DISCUSSION

Using ^{99m}Tc-Cy5-MAS$_3$, we labeled SPZ and assessed their motility *in vitro* and their dissemination *in vivo*. The fluorescent signature of the tracer was used to confirm the labeling of SPZ by microscopy and flow cytometry. The radioactive signature enabled the quantitative assessment of the distribution of SPZ in a murine model. This study revealed that following intravenous injection, live SPZ mainly migrate towards the liver, whereas non-viable SPZ partly relocate to the lungs. These results indicate that SPZ viability plays a role in overcoming the physical barrier of lung microvasculature.

The design of the hybrid tracer was based on the previous developed fluorescent tracer Cy5-methyl-methyl, now extended with a chelate for technetium[24]. So far, besides Cy5-methyl-methyl only CFSE (covalently couples to intracellular free amines) has been used to fluorescently label live SPZ for tracking and no radioactive tracers suitable to label SPZ have been reported[31]. The use of a hybrid tracer proved to be valuable in providing both the envisaged radiolabeling of SPZ needed for whole-body tracking and the microscopic and flow cytometric validation of the labeling. ^{99m}Tc-Cy5-MAS$_3$ was 1) able to accumulate intracellularly and had a low efflux rate, 2) nontoxic for SPZ and 3) detectable over a longer period of time. First, the tracer accumulated inside the SPZ resulting in a concentration of radioactivity which was high enough for a biodistribution study in a murine model and which was stable for at least the 2 hr measured in this study. This sensitivity needed to quantify the biodistribution of SPZ in mice has not been achieved by other techniques applied so far, such as bioluminescence-based imaging or PCR[32]. Moreover, the fitness assays did not reveal significant toxic effects of the labeling with ^{99m}Tc-Cy5-MAS$_3$ to SPZ at the dose used; although the infectivity may have been somewhat decreased (albeit non-significantly) based on infection assays *in vitro* and *in vivo*. Lastly, ^{99m}Technetium, the most commonly utilized radionuclide due to favorable properties such as a 6-hour half-life[33], enabled SPZ tracking 2 hr post injection and might support longitudinal tracking up to 24 hr in future studies if the initial tracer uptake is sufficiently high.

The lack of specificity of ^{99m}Tc-Cy5-MAS$_3$ for SPZ was a disadvantage, because the SPZ sample which was labeled *ex vivo* was contaminated with SGM. This resulted *in vivo* in the presence of labeled SGM and free tracer released from SGM which complicated the interpretation of the absolute SPZ biodistribution data. These findings are in line with the fact that tracer release from dead cells is commonly noted as a pitfall of *ex vivo* labeling methods[22]. Nevertheless, the fast hepatic clearance of free tracer facilitated the separation of signal from free tracer (in the gall bladder and intestine) and SPZ, which could be used for a reliable assessment of the relative SPZ biodistribution. The use of purified SPZ could in the future solve the problem of SGM contamination[34].

The biodistribution results of SGM revealed a preference of SGM to relocate to the lungs and liver. The varying SGM particle size (around an average of ~2 µm) may explain the distribution of these particles over the lungs and the liver, smaller particles tend to be cleared via the liver, while bigger particles end up in the lungs[35-37]. Interestingly, the biodistribution of the SPZ was impacted by their viability with a lower liver-to-lungs distribution for non-viable SPZ. Based on the size of SPZ (crescent-shaped, length: 8-14 µm), it is not that surprising that part of them get physically trapped in lung capillaries (typical diameter mouse capillaries: ~4 µm[38]). These results suggest that SPZ viability, and probably their motility, plays a key role in passing the lungs to reach hepatocytes to complete their life cycle[39]. Using confocal microscopy, we observed motile SPZ in rodent lung tissue; future studies should investigate how this motility facilitates lung passage.

We are the first to demonstrate the presence and passage of SPZ through the lungs. Lung passage of malaria SPZ has not been previously investigated. However, particles of similar size, such as intravenously injected albumin-based microspheres (diameter: 18 µm) are used as a clinical tool to visualize lung perfusion because of their capacity to get trapped in the lungs. Also for monocytes and dendritic cells it has been shown that they first accumulate in the lungs before getting distributed to other organs[37, 40-42]. These studies support the notion that the microvasculature of the lungs can provide a physical barrier for particles, amongst which SPZ, to passage. Interestingly, SPZ-immune cell interactions in the lungs have not yet been considered in the field of malaria vaccine development.

Further SPZ biodistribution and immunological studies are needed to provide valuable insights into the spatial and temporal dynamics of the migration of vaccine SPZ which are attenuated (e.g. genetically attenuated, radiation attenuated) or administered via different routes (e.g. intravenous, intradermal, subcutaneous)[11] and the role of the lung-trapped SPZ in the induction of the overall immune response. This would help understand what would be the most optimal means of delivering these complex vaccines, critical viability thresholds and the sites where essential immune interactions take place.

In conclusion, development of a hybrid tracer enabled the first radioactivity-based assessment of the SPZ biodistribution in mice. Despite the need for further technical improvements, these first results provided new insights into SPZ dissemination *in vivo*. Moreover, the presented method allows monitoring of the spatial and temporal dynamics of SPZ migration throughout the host post injection, providing critical information for the improvement of whole SPZ vaccine potency.

Acknowledgments: We would like to thank ing. J. Ramesar and dr. C.J. Janse for support with the mosquito infection.

REFERENCES

1. World Health, O., World malaria report 2021. 2021, Geneva: World Health Organization.
2. de Korne, C., et al., Clustering and erratic movement patterns of syringe-injected versus mosquito-inoculated malaria sporozoites underlie decreased infectivity. Msphere, 2021. 6(2): p. e00218-21.
3. Frischknecht, F. and K. Matuschewski, Plasmodium sporozoite biology. Cold Spring Harbor Perspectives in Medicine, 2017. 7(5): p. a025478.
4. Medica, D.L. and P. Sinnis, Quantitative dynamics of Plasmodium yoelii sporozoite transmission by infected anopheline mosquitoes. Infection and immunity, 2005. 73(7): p. 4363-4369.
5. Sinnis, P. and A. Coppi, A long and winding road: the Plasmodium sporozoite's journey in the mammalian host. Parasitology international, 2007. 56(3): p. 171-178.
6. Richie, T.L., et al., Progress with Plasmodium falciparum sporozoite (PfSPZ)-based malaria vaccines. Vaccine, 2015. 33(52): p. 7452-61.
7. Roestenberg, M., et al., A double-blind, placebo-controlled phase 1/2a trial of the genetically attenuated malaria vaccine PfSPZ-GA1. Sci Transl Med, 2020. 12(544).
8. Sissoko, M.S., et al., Safety and efficacy of a three-dose regimen of Plasmodium falciparum sporozoite vaccine in adults during an intense malaria transmission season in Mali: a randomised, controlled phase 1 trial. The Lancet Infectious Diseases, 2022. 22(3): p. 377-389.
9. Epstein, J.E., et al., Live attenuated malaria vaccine designed to protect through hepatic CD8(+) T cell immunity. Science, 2011. 334(6055): p. 475-80.
10. Seder, R.A., et al., Protection against malaria by intravenous immunization with a nonreplicating sporozoite vaccine. Science, 2013. 341(6152): p. 1359-65.
11. Itsara, L.S., et al., The development of whole sporozoite vaccines for Plasmodium falciparum malaria. Frontiers in immunology, 2018. 9: p. 2748.
12. Phillips, M.A., et al., Malaria. Nature Reviews Disease Primers, 2017. 3(1): p. 17050.
13. Amino, R., et al., Quantitative imaging of Plasmodium transmission from mosquito to mammal. Nat Med, 2006. 12(2): p. 220-4.
14. Yamauchi, L.M., et al., Plasmodium sporozoites trickle out of the injection site. Cellular microbiology, 2007. 9(5): p. 1215-1222.
15. Hopp, C.S., et al., Longitudinal analysis of Plasmodium sporozoite motility in the dermis reveals component of blood vessel recognition. Elife, 2015. 4.
16. Vanderberg, J.P. and U. Frevert, Intravital microscopy demonstrating antibody-mediated immobilisation of Plasmodium berghei sporozoites injected into skin by mosquitoes. Int J Parasitol, 2004. 34(9): p. 991-6.
17. Winkel, B.M.F., et al., Quantification of wild-type and radiation attenuated Plasmodium falciparum sporozoite motility in human skin. Scientific Reports, 2019. 9.
18. Ploemen, I.H., et al., Plasmodium liver load following parenteral sporozoite administration in rodents. Vaccine, 2013. 31(34): p. 3410-3416.
19. Vaughan, A.M., et al., A Plasmodium parasite with complete late liver stage arrest protects against preerythrocytic and erythrocytic stage infection in mice. Infection and immunity, 2018. 86(5): p. e00088-18.
20. Perrin, J., et al., Cell tracking in cancer immunotherapy. Frontiers in Medicine, 2020. 7: p. 34.
21. Rodriguez-Porcel, M., et al., Cell tracking and the development of cell-based therapies: a view from the Cardiovascular Cell Therapy Research Network. JACC: Cardiovascular Imaging, 2012. 5(5): p. 559-565.
22. Kurebayashi, Y., P.L. Choyke, and N. Sato, Imaging of cell-based therapy using 89Zr-oxine ex vivo cell labeling for positron emission tomography. Nanotheranostics, 2021. 5(1): p. 27.
23. Roca, M., et al., Guidelines for the labelling of leucocytes with 111In-oxine. European journal of nuclear medicine and molecular imaging, 2010. 37(4): p. 835-841.
24. Winkel, B.M.F., et al., A tracer-based method enables tracking of Plasmodium falciparum malaria parasites during human skin infection Theranostics, 2019. 9(10): p. 2768-2778.
25. Hensbergen, A.W., et al., Evaluation of asymmetric orthogonal cyanine fluorophores. Dyes and Pigments, 2020. 183: p. 108712.
26. Robu, S., et al., Preclinical evaluation and first patient application of 99mTc-PSMA-I&S for SPECT imaging and radioguided surgery in prostate cancer. Journal of Nuclear Medicine, 2017. 58(2): p.

235-242.
27. Haeberlein, S., et al., Protective immunity differs between routes of administration of attenuated malaria parasites independent of parasite liver load. Sci Rep, 2017. 7(1): p. 10372.
28. de Korne, C.M., et al., Regulation of Plasmodium sporozoite motility by formulation components. Malaria Journal, 2019. 18.
29. Schindelin, J., et al., Fiji: an open-source platform for biological-image analysis. Nature Methods, 2012. 9(7): p. 676-682.
30. Welling, M., et al., Interventional nuclear medicine:"click" chemistry as an in vivo targeting strategy for imaging microspheres and bacteria. Biomaterials Science, 2021. 9(5): p. 1683-1690.
31. Zhou, C., et al., Laser mimicking mosquito bites for skin delivery of malaria sporozoite vaccines. Journal of Controlled Release, 2015. 204: p. 30-37.
32. Ploemen, I.H.J., et al., Visualisation and Quantitative Analysis of the Rodent Malaria Liver Stage by Real Time Imaging. Plos One, 2009. 4(11).
33. Moreira, M.L., et al., In vivo tracking of cell therapies for cardiac diseases with nuclear medicine. Stem cells international, 2016. 2016.
34. Hoffman, S.L. and T.C. Luke, Apparatuses and methods for the production of haematophagous organisms and parasites suitable for vaccine production. 2014, Google Patents.
35. He, Q., et al., In vivo biodistribution and urinary excretion of mesoporous silica nanoparticles: effects of particle size and PEGylation. small, 2011. 7(2): p. 271-280.
36. Ogawara, K.-i., et al., Hepatic uptake of polystyrene microspheres in rats: effect of particle size on intrahepatic distribution. Journal of Controlled Release, 1999. 59(1): p. 15-22.
37. Stephens, R.W., et al., 99mTc-radiolabeled composites enabling in vivo imaging of arterial dispersal and retention of microspheres in the vascular network of rabbit lungs, liver, and liver tumors. International Journal of Nanomedicine, 2019. 14: p. 889.
38. Müller, B., et al. High-resolution tomographic imaging of microvessels. in Developments in X-ray Tomography VI. 2008. SPIE.
39. Ejigiri, I. and P. Sinnis, Plasmodium sporozoite–host interactions from the dermis to the hepatocyte. Current opinion in microbiology, 2009. 12(4): p. 401-407.
40. Ritchie, D., et al., In vivo tracking of macrophage activated killer cells to sites of metastatic ovarian carcinoma. Cancer Immunology, Immunotherapy, 2007. 56(2): p. 155-163.
41. Spa, S.J., et al., A supramolecular approach for liver radioembolization. Theranostics, 2018. 8(9): p. 2377.
42. Van Hemert, F.J., et al., Labeling of autologous monocytes with 99mTc–HMPAO at very high specific radioactivity. Nuclear medicine and biology, 2007. 34(8): p. 933-938.

SUPPLEMENTARY INFORMATION

1. Tracer synthesis
2. Overview biodistribution results (Sup. Figure S1)
3. Labeling of and tracer release from salivary gland material (Sup. Figure S2)
4. Validation of SPZ presence in organs by PCR (Sup. Figure S3)
5. Validation of SPZ presence in organs by confocal microscopy (Sup. Figure S4)
6. Estimation of SGM particle size (Sup. Figure S5)

1. Tracer synthesis

General

All chemicals and solvents were obtained from commercial sources and used without further purification. Dimethylformamide (DMF), dichloromethane (DCM) and dimethylsulfoxide (DMSO) were dried with 4 Å molecular sieves, unless stated otherwise. Column chromatography was performed with 40–63 µm silica from Screening Devices. Dry column vacuum chromatography (DCVC) was performed as published by Pedersen *et al*. [1] with 15–40 µm silica and Hyflo Supercell Celite from Fisher Scientific. High-performance liquid chromatography (HPLC) was performed with a Waters HPLC system using either a 1525EF or 2545 pump and a 2489 UV/VIS detector. For preparative HPLC either a Dr. Maisch GmbH Reprosil-Pur 120 C18-AQ 10 µm (250 × 20 mm) column or a XBridge Prep C8 10 µm OBD 250 × 30 mm column was used with a gradient of 0.1% trifluoro acetic acid (TFA) in H_2O/acetonitrile (CH_3CN) 95:5 to 0.1% TFA in H_2O/CH_3CN 5:95 in 40 min (12 or 25 ml/min, respectively) was employed. For semi-preparative HPLC a Dr. Maisch GmbH Reprosil-Pur C18-AQ 10 µm (250 × 10 mm) column was used and a gradient of 0.1% TFA in H_2O/CH_3CN 95:5 to 0.1% TFA in H_2O/CH_3CN 5:95 in 40 min (5 ml/min) was employed. For analytical HPLC a Dr. Maisch GmbH Reprosil-Pur C18-AQ 5 µm (250 × 4.6 mm) column was used and a gradient of 0.1% TFA in H_2O/CH_3CN 95:5 to 0.1% TFA in H_2O/CH_3CN 5:95 in 40 min (1 ml/min) was employed. High-resolution mass spectrometry (HRMS) was performed on a Waters Acquity H-class UPLC using a Acquity UPLC BEH C18 1.7 µm (2.1 × 50 mm) column with a gradient of 0.1% FA in H_2O/CH_3CN 98:2 to 0.1% FA in H_2O/CH_3CN 60:40 in 1.8 min (0.6 ml/min) coupled to a high-resolution Waters XEVO G2S-XTOF Mass Spectrometer. Low-resolution mass spectrometry (LRMS) was performed using a Bruker Microflex matrix-assisted laser desorption ionization time-of-flight (MALDI-TOF) mass spectrometer. ^{1}H and ^{13}C NMR were performed on a Bruker Ascend 850 (850 MHz) equipped with a CryoProbe in deuterated solvents. Absorbance spectra were recorded using an Ultrospec 2100 pro from Amersham Biosciences. Fluorescence spectra were recorded using a PerkinElmer LS-55 fluorescence spectrometer.

Synthesis mercaptoacetyltriserine (mas_3)

D-Ser(tBu)-WANG (3.0 g, 720 µmol) was swollen in DCM (20 ml) and washed 4 times with

DCM (20 ml). mas_3 was synthesized using standard Fmoc-based SPPS procedures using two cycles of Fmoc-D-(Ser(tBu)-OH (4 eq), PyBOP (4 eq) and N-methylmorpholine (5 eq) at RT for 2 hr and one cycle of s-acetylthioacetic acid (4 eq), PyBOP (4 eq) and N-methylmorpholine (5 eq) at RT for 2 hr. The resin was cleaved by shaking with TFA/H_2O (95:5; 20 ml) for 90 minutes and precipitating in ice cold MTBE/Et_2O (300 ml). The precipitate was washed with ice cold MTBE/Et_2O twice before drying *in vacuo*. The crude compound was purified using prep-HPLC. Lyophilization then yielded the title compound as a white fluffy solid (145 mg, 51%). 1H NMR (850 MHz, D_2O) δ 4.52 (t, J = 5.1 Hz, 1H), 4.50 (t, J = 4.4 Hz, 1H), 4.47 (t, J = 5.4 Hz, 1H), 3.74 (dd, J = 5.2, 11.6 Hz, 1 H), 3.76 (dd, J = 4.3, 12.1 Hz, 1 H), 3.78 (dd, J = 6.6, 11.8 Hz, 1 H), 3.79 (dd, J = 6.0, 11.9 Hz, 1 H), 3.80 (dd, J = 5.8, 11.8 Hz, 1 H), (dd, J = 4.9, 11.8 Hz, 1 H), 3.72 (q, J = 15.6 Hz, 2H), 2.37 (s, 3H). ^{13}C NMR (214 MHz, D_2O) δ 200.72, 174.08, 172.77, 172.47, 172.32, 62.03, 62.00, 61.93, 61.85, 56.84, 56.38, 55.93, 33.72, 30.41. HRMS m/z calculated for $C_{13}H_{21}N_3O_9S$ 396.1077, measured 396.1092 (3.79 ppm).

Synthesis Cy5-AmineC4Phth-Methyl

Indole-AmineC4Phth (1479 mg, 3.35 mmol; [2]) and malonaldehyde dianilide HCl (954 mg, 3.69 mmol) were dissolved in Ac2O/AcOH (1:1; 40 ml) and stirred at 60 °C overnight. The mixture was subsequently heated to 120 °C for 60 min and then cooled down to RT. Precipitation in and washing with Et_2O yielded the crude hemicyanine which was dissolved in DMF/DCM (1:1, 40 mL) and added to swollen WANG resin (1065 mg, 1.78 mmol). After coupling for 60 minutes, the resin was washed with DMF/DCM mixtures. Indole-methyl (213 mg, 0.84 mmol; [3]) was dissolved in pyridine/Ac2O (3:1, 40 ml) and added to the resin. The mixture was shaken overnight at RT before collecting the filtrate. The obtained crude was purified by DCVC and prep-HPLC. Lyophilization yielded the title compound as a blue solid. ^1H NMR (850 MHz, DMSO) δ 8.30 (q, J = 14.0 Hz, 2H), 7.87 (dd, J = 5.4, 3.0 Hz, 2H), 7.82 (dd, J = 5.4, 3.0 Hz, 2H), 7.62 (d, J = 7.3 Hz, 1H), 7.60 (d, J = 7.2 Hz, 1H), 7.43 – 7.38 (m, 3H), 7.36 (td, J = 3.6, 0.4 Hz, 1H), 7.26 (ddd, J = 7.4, 5.9, 2.3 Hz, 1H), 7.21 (td, J = 7.3, 0.7 Hz, 1H), 6.52 (t, J = 12.3 Hz, 1H), 6.28 (t, J = 13.0 Hz, 2H), 4.11 (m, 2H), 3.62 (s, 5H), 1.71 (br. s, 4H), 1.68 (s, 6H), 1.66 (s, 6H). ^{13}C NMR (214 MHz, DMSO) δ 173.45, 172.37, 168.11, 158.11, 157.95, 154.18, 154.00, 142.79, 142.09, 141.10, 141.02, 134.47, 134.39, 131.57, 128.40, 125.33, 124.83, 124.56, 123.10, 123.03, 122.44, 122.36, 111.15, 111.03, 103.49, 102.99, 48.93, 48.81, 42.85, 39.88, 39.78, 37.04, 31.15, 27.19, 26.99, 25.13, 24.21. HRMS m/z calculated for $C_{38}H_{40}N_3O_2^+$ 570.3121, measured 570.3107 (2.45 ppm).

Synthesis Cy5-AmineC4-Methyl

Cy5-Methyl-AmineC4Phth (60 mg, 105 µmol) was dissolved in methylamine (33 wt% in EtOH, 25 ml) and stirred at RT. After 3 hours, the reaction was complete and volatiles were removed *in vacuo*. The crude product was purified by prep-HPLC. Lyophilization yielded the title compound as a blue solid (40.9 mg, 88%). ^1H NMR (850 MHz, MeOD) δ 8.27 (q, J = 13.6

Hz, 2H), 7.51 (d, J = 7.3 Hz, 1H), 7.49 (d, J = 7.0 Hz, 1H), 7.43 (td, J = 7.9, 1.1 Hz, 1H), 7.40 (td, J = 7.9, 1.1 Hz, 1H), 7.33 (d, J = 7.9 Hz, 1H), 7.30 (d, J=8.0 Hz, 1 H), 7.29 (td, J=7.4, 0.7 Hz, 1 H), 7.25 (td, J = 7.4, 0.5 Hz, 1H), 6.64 (t, J = 12.4 Hz, 1H), 6.30 (t, J = 12.5, 2H), 4.16 (t, J = 7.4 Hz, 2H), 3.65 (s, 3H), 2.99 (t, J = 7.6 Hz, 2H), 1.94 – 1.85 (m, 2H), 1.84 – 1.77 (m, 2H), 1.74 (s, 6H), 1.73 (s, 6H). ^{13}C NMR (214 MHz, MeOD) δ 176.01, 174.16, 174.13, 155.99, 155.93, 155.35, 155.30, 144.16, 143.57, 142.65, 142.50, 129.78, 129.75, 126.75, 126.71, 126.55, 126.06, 123.47, 123.32, 112.08, 111.74, 104.87, 103.91, 50.70, 50.67, 50.41, 44.14, 40.38, 31.61, 28.01, 27.70, 26.02, 25.53. HRMS m/z calculated for $C_{30}H_{48}N_3^+$ 440.3066, measured 440.3087 (4.77 ppm).

Synthesis Cy5-AmineC4.mas$_3$-Methyl

mas$_3$ (27 mg, 68 µmol), 1-[bis(dimethylamino)methylene]-1H-1,2,3-triazolo[4,5-b] pyridinium 3-oxide hexafluorophosphate (26 mg, 68 µmol) and N-methylmorpholine (34 mg, 340 µmol) were dissolved in DMSO (2 ml), and the solution immediately turned yellow. This solution was then added to Cy5-AmineC4-Methyl (30 mg, 68 µmol) and the reaction mixture was stirred at RT for 25 min. A mixture of H_2O/MeCN (85/15, 8 ml) with 0.1% TFA was added and the crude product was purified by prep-HPLC. Lyophilization yielded the product as a blue solid (30 mg, 54%). ^{1}H NMR (850 MHz, DMSO) δ 8.37 – 8.29 (m, 3H), 8.15 (dd, J = 13.0, 7.2 Hz, 1H), 7.90 (d, J = 7.9 Hz, 1H), 7.87 (d, J = 7.9 Hz, 1H), 7.62 (d, J = 7.4 Hz, 1H), 7.61 (d, J = 7.4 Hz, 1H), 7.43 – 7.36 (m, 4H), 7.25 (t, J = 7.6 Hz, 1H), 7.24 (t, J = 7.4 Hz, 1H), 6.56 (t, J = 12.0 Hz, 1H), 6.26 (d, J = 13.8 Hz, 1H), 5.19 (t, J = 4.9 Hz, 1H), 5.14 (t, J = 4.9 Hz, 1H), 4.88 (t, J = 4.7 Hz, 1H), 4.36 (dt, J = 7.6, 6.0 Hz, 1H), 4.30 (q, J = 6.36 Hz, 1H), 4.20 (dt, J = 8.0, 5.5 Hz, 1H), 4.07 (t, J = 7.1 Hz, 2H), 3.68 (s, 2H), 3.60 (br. s, 5H), 3.57 – 3.49 (m, 2H), 3.16 (sextet, J = 7.0 Hz, 1H), 3.08 (sextet, J = 6.4 Hz, 1H), 2.33 (d, J = 4.8 Hz, 3H), 1.73 – 1.62 (m, 14H), 1.53 (p, J = 6.5 Hz, 2H). ^{13}C NMR (214 MHz, DMSO) δ 194.57, 194.56, 173.25, 172.49, 172.47, 170.38, 170.20, 170.02, 169.99, 169.69, 169.67, 167.23, 167.20, 154.12, 154.04, 142.81, 142.01, 141.09, 141.05, 128.48, 128.39, 125.45, 124.75, 124.64, 122.44, 122.35, 111.15, 111.07, 103.35, 103.33, 103.11, 61.70, 61.46, 61.42, 61.36, 61.34, 55.76, 55.66, 55.54, 55.39, 55.33, 55.24, 48.87, 43.16, 39.98, 39.88, 39.78, 38.04, 37.99, 32.52, 32.50, 31.34, 31.08, 30.13, 27.21, 27.02, 26.25, 26.18, 24.14. HRMS m/z calculated for $C_{43}H_{57}N_6O_8S^+$ 817.3959, measured 817.3946 (1.59 ppm).

References

1. D.S. Pedersen *et al*. Synthesis 2001. DOI: 10.1055/s-2001-18722
2. A.W.H. Hensbergen *et al*. J. Nucl. Med. 2020. DOI: 10.2967/jnumed.119.233064
3. A. Bunschoten *et al*. Bioconjug. Chem. 2016 DOI: 10.1021/acs.bioconjchem.6b00093

2. Overview biodistribution results

In this study the biodistribution was determined of: 1) the free tracer ^{99m}Tc-Cy5 -AmineC4.

MAS_3-Methyl (abbreviated as ^{99m}Tc-Cy5-MAS_3), 2) SGM labeled with ^{99m}Tc-Cy5-MAS_3, 3) live SPZ labeled with ^{99m}Tc-Cy5-MAS_3 and 4) non-viable SPZ ^{99m}Tc-Cy5-MAS_3. An overview of the results is shown in Sup. Figure S1, which includes the %ID and %ID/g determined for 16 different tissues.

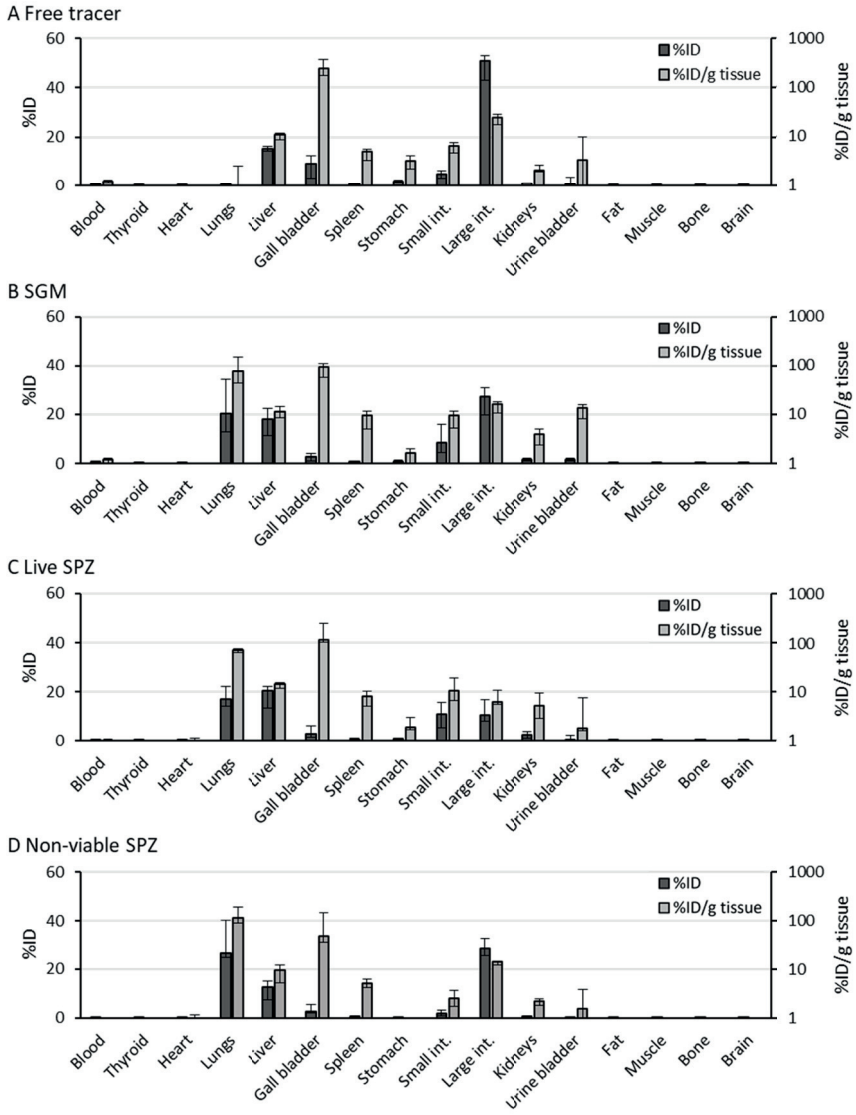

Sup. Figure S1 Biodistribution results. A-D) The biodistribution of the free tracer ^{99m}Tc-Cy5-MAS_3 (A), SGM labeled with ^{99m}Tc-Cy5-MAS_3 (B), live SPZ labeled with ^{99m}Tc-Cy5-MAS_3 (C) and non-viable SPZ labeled with ^{99m}Tc-Cy5-MAS_3 (D) measured 2 hr post injection, plotted as the median percentage of injected dose (%ID; depicted in dark grey) and the %ID per gram tissue (&ID/g tissue; depicted in light gray) per organ including error bars representing the inter quartile range.

3. Labeling of and tracer release from SGM

Flow cytometric analysis of the labeled SPZ sample revealed that besides the SPZ (42 ± 9 % of the detected particles) also the present SGM was labeled, on average the mean fluorescent intensity of the SGM was 1.9 fold higher compared to the SPZ (Sup. Figure S2). Over time, tracer was released from SGM which led to a 1.6 fold decrease in mean fluorescent intensity in 2 hr time (Sup. Figure S2).

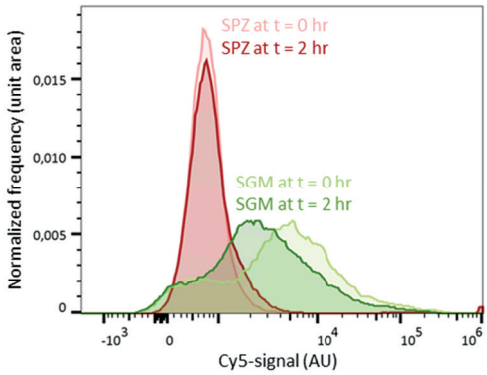

Sup. Figure S2 Labeling of sporozoites and SGM.
The Cy5-signal in labeled SPZ (depicted in red) and labeled SGM (depicted in green) was measured at t = 0 hr (depicted in light color) and at t = 2hr (depicted in dark color). The fold change in mean fluorescence intensity over time was 1.0 for SPZ and 1.6 for SGM.

4. Validation of SPZ presence in organs by PCR

To interpret the biodistribution results, more specifically to estimate the share of SPZ in the mixed distribution of SPZ, SGM and free tracer, the assumption was made that the radioactive signal found back in the tracer clearance organs (intestines + gall bladder) came from free tracer released from the SGM. This assumption was supported by qRT-PCR analysis of the different organs from mice used for the biodistribution study whereby no clearance organs positive for *Plasmodium* DNA were found, whereas occasional positive signals in liver and lungs were found (Sup. Figure S3).

Methods

Parasite burden in lungs, liver, skin and clearance organs (intestines and gall bladder) was measured by quantitative real-time reverse transcription-polymerase chain reactions (qRT-PCR). The DNA was extracted from the frozen tissues using the QIAamp DNA Micro Kit (Qiagen) following the manufacturer's instruction. Amplification reactions of each DNA sample were performed in PCR plates (hard-shell PCR plate, #HSP9645; Bio-Rad), in a volume of 25 µl containing 12.5 µl PCR buffer (HotstarTaq mastermix; Qiagen), 0.5 µl MgCl2 (25mM), Plasmodium-specific forward and reverse primer (12.5 pmol; Plas-7F 5'-GTTAAGGGAGTGAAGACGATCAGA-3' and Plas-171R 5'-AACCCAAAGACTTTGATTTCTCATAA-3'; Sigma-Aldrich), PhHV-specific forward and reverse primer (15 pmol; PhHV-267S 5'-GGGCGAATCACAGATTGAATC -3' and PhHV-337AS

5'-GCGGTTCCAAACGTACCAA -3'; Biolegio), Plasmodium-specific FAM10 labeled detection probe (2.5 pmol; PP FAM 5'-ACCGTCGTAATCTTAACC-3'; Biolegio), PhHV-specific Cy5 double-labeled detection probe (1.25 pmol; PhHV-305TQCy55'-TTTTTATGTGTCCGCCACCATCTGGATC-3'-BHQ2; Biolegio) and 5 µl of the DNA sample (20 ng/µl, dilution factor: 10x). Amplification consisted of 15 min at 95°C followed by 50 cycles of 15 s at 95°C, 30 s at 60°C, and 30 s at 72°C. Amplification, detection, and analysis were performed with the CFX96TM real-time PCR detection system (Bio-Rad).

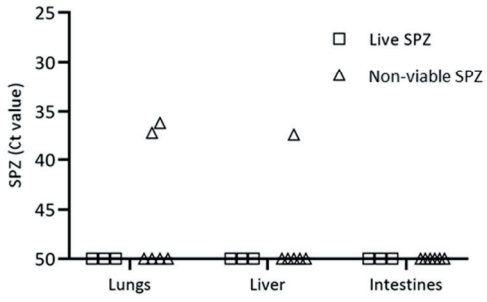

Sup. Figure S3 PCR on organs to assess the presence of sporozoites.
The Ct (cycle threshold) value obtained by qRT-PCR for the lungs, livers and intestines of the mice used for the biodistribution study was plotted. A Ct-value of 50 meant that no *Plasmodium* DNA was detected.

5. Validation of sporozoite presence in organs by confocal microscopy

To validate the presence of SPZ in the lungs and the liver, these organs were microscopically examined 2 hr after intravenous injection of SPZ labeled with Cy5-MAS_3. Following injection of live SPZ, a few SPZ were found back in the lungs and the majority was found back in the liver (Sup. Figure S4A). Following injection of non-viable SPZ, we could not find back SPZ in neither the lungs and the liver, which suggested that the fluorescent signal had disappeared probably due to disintegration of the SPZ. Video recording of live SPZ in lung tissue showed that the SPZ were able to move in this environment (Sup. Figure S4B).

Methods

To validate the SPZ presence in different organs by confocal microscopy, $1.0*10^6$ live or non-viable SPZ labeled with Cy5-MAS_3 were intravenously injected into the tail vein of mice. At 2 hr post-injection the mice were euthanized, lungs and liver were sliced and mounted in a confocal dish. To assess SPZ motility in lung tissue, $1.0*10^6$ live SPZ were injected via the heart into the lung circulation directly after euthanization and subsequently the lungs were sliced and mounted in a confocal dish. Images and movies (2 min) were recorded as a Z-stack covering a total depth of 30 µm. An Andor Dragonfly 500 spinning disk confocal on a Leica DMi8 microscope (Oxford Instruments) with a 40x objective (HCX PL APO 40x/1.30 OIL) was used. The mCherry expressed by the SPZ was excited with the 561 nm laser and the 637 nm laser was used to excite Cy5. Maximum projections of the Z-stacks were generated using Fiji software.

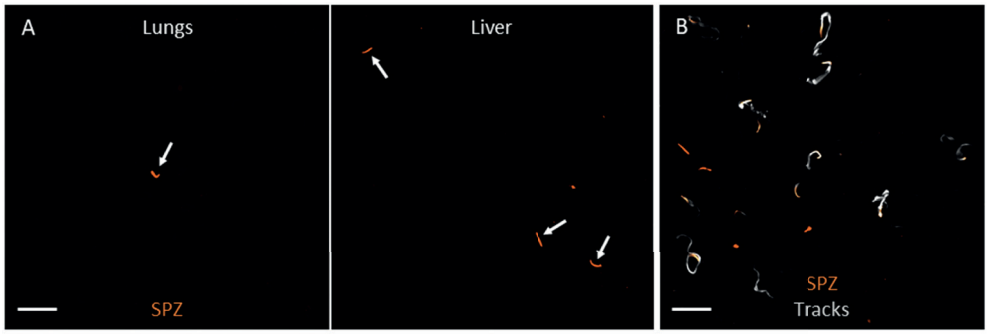

Sup. Figure S4 Sporozoite presence in lungs and liver. A) Confocal images of SPZ in lung tissue (left) and liver tissue (right) (depicted in orange and annotated with a white arrow). B) A maximum projection of a movie (2 min) of SPZ in lung tissue. The SPZ at t= 0 min are shown in orange and the tracks of the moving SPZ are shown in grey. Scale bar: 30 µm.

6. Estimation of SGM particle size

To estimate the size of the SGM particles, flow cytometric analysis was used whereby SGM was compared to 2, 3 and 10 µm beads based on FSC intensity which is proportional to particle size. The median FSC intensities of the beads were: $8.5*10^4$ (IQR: $7.5*10^4$-$9.7*10^4$) for the 2 µm beads, $7.3*10^5$ (IQR: $7.1*10^5$-$7.5*10^5$) for the 3 µm beads and $2.4*10^6$ (IQR: $2.4*10^6$-$2.4*10^6$) for the 10 µm beads (Fig. S5). The median FSC intensity of the SGM came closest to the 2 µm beads, however the IQR was much larger compared to the beads (median FSC intensity SGM: $1.2*10^5$ (IQR: $8.0*10^4$-$2.1*10^5$)) (Fig. S5). So, the SGM particle size varied substantially, but was on average ~2 µm.

Methods

To estimate the SGM particle size, the forward scatter (FSC) intensity of SGM was assessed using a flow cytometer (Cytek Aurora; Cytek Biosciences) and compared to the FSC intensity of 2 µm and 3 µm CS&T research beads (BD Biosciences) and 10 µm FITC labeled micro particles based on melamine resin (Merck). The data was analyzed using the FlowJo software (FlowJo LLC). SGM and the CS&T beads were selected by gating based on a forward versus sideward scatterplot and the 10 µm beads were selected by gating on FITC-positive events.

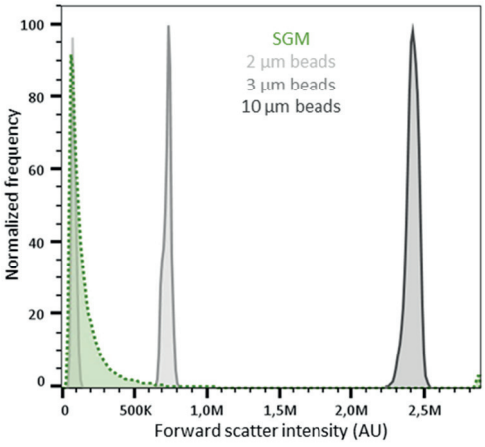

Sup. Figure S5 SGM particle size.
Flowcytometric analysis of the mean FSC intensity of SGM (depicted in green) which was compared to the mean FSC intensity of 2 µm, 3 µm and 10 µm beads (depicted in grey). The frequency of the events was normalized to the mode.